

Development of a one-dimensional detector for the study of explosions with a synchrotron radiation beam†

Vladimir Aulchenko, Pavel Papushev, Sergey Ponomarev, Lev Shekhtman* and Vladimir Zhulanov

Budker Institute of Nuclear Physics, 11 Lavrentiev Avenue, Novosibirsk 630090, Russia. E-mail: l.i.shekhtman@inp.nsk.su

Investigations of fast dynamic processes with the help of synchrotron radiation allow an understanding of the properties of short-lifetime states of materials at very high temperatures and pressures. Detectors for such studies have to be able to detect X-ray photons from each electron bunch separately with a position resolution of about 0.1 mm. A prototype of a detector (DIMEX) for the imaging of explosions at a synchrotron radiation beam is described here. A spatial resolution of $\sim 300 \mu\text{m}$ and a time resolution of $\sim 100 \text{ ns}$ is demonstrated with a synchrotron radiation beam from the VEPP-3 2 T wiggler at an electron beam energy of 2 GeV. Results of the first projective imaging and SAXS experiments are presented.

Keywords: imaging; detectors; explosions; time resolution.

1. Introduction

Synchrotron radiation has been shown to be a powerful tool for studying very fast physical and chemical processes at high temperatures and pressures during explosions (Aleshaev *et al.*, 2001; Tolochko *et al.*, 2001). Very fast pulses of synchrotron light produced by short electron bunches allow imaging of the development of the detonation wave as well as fluctuations of electron density within the volume of the exploding materials. Such experiments require an exceptional set of detector parameters. In order to view images from different electron bunches independently, the time resolution of the detector has to be smaller than the bunch-crossing time. For the VEPP-3 storage ring this time is 250 ns in single-bunch mode. A spatial resolution of $\sim 0.1 \text{ mm}$ allows one to view the shock-wave structure in projective imaging experiments. A detection efficiency of more than 50% is very desirable in order to obtain good photon statistics. Finally, an efficient imaging at such a frame rate requires a very high photon rate capability of 10^{10} – $10^{11} \text{ s}^{-1} \text{ mm}^{-2}$. At such a photon rate the detector can work only in charge integrating mode. Another restriction arises from the requirement of the high frame rate. Storage of a frame within $\sim 100 \text{ ns}$ is quite difficult. Thus, raw data from the detector have to be stored in analogue form during the experiment. After the end of the measurement, data can be digitized and stored in a final storage area without time constraints.

In the present paper we introduce a new detector (DIMEX) for the imaging of fast dynamic processes and explosions with a synchrotron radiation beam. The detector is based on an ionization chamber with charge collection to a microstrip structure coupled to an ASIC with integrators and a fast analogue memory.

2. Detector design

DIMEX consists of an ionization chamber with a $100 \mu\text{m}$ pitch microstrip readout. The chamber is filled with XeCO_2 (80–20%) at

7 atm. A high-voltage drift electrode pushes the electron component of the primary ionization to the readout strips (Fig. 1). A gas electron multiplier (GEM) (Sauli, 1997), stretched at a distance of 1 mm above the microstrip structure, shields the ionic component of the primary ionization. The distance between the drift electrode and the GEM foil is 2 mm.

A narrow beam of synchrotron radiation ($\sim 1 \text{ mm}$ high) is transmitted or scattered by the sample. From there the synchrotron radiation enters the conversion volume between the drift electrode and the GEM. The electronic component of the primary ionization drifts towards the GEM, penetrates the holes and induces charge on the strips. The positive ions move towards the drift electrode and are collected. Owing to the shielding of the GEM they do not induce charge to the readout strips. GEM is a microstructure consisting of regularly punched holes in an insulating (kapton) film, clad on both sides with thin copper layers. The foil thickness is $50 \mu\text{m}$, the pitch of the holes is $140 \mu\text{m}$ and their diameter is $\sim 80 \mu\text{m}$. Thus the GEM acts as a Frisch grid, providing additional possibilities, *i.e.* by choosing an appropriate voltage between the metal layers on the sides of the GEM we can flexibly tune the fraction of charge penetrating the foil or amplify it.

Readout strips are connected to the input pads of an APC128 ASIC (Horisberger & Pitzl, 1993). The ASIC consists of 128 channels with low-noise integrators at the input and a 32-cell analogue pipeline. All 128 channels can be read out in series through an analogue multiplexer (Fig. 2).

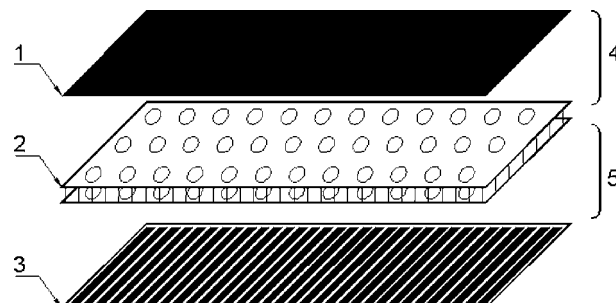


Figure 1
Schematic design of the sensitive part of DIMEX. 1, drift electrode; 2, GEM; 3, microstrip structure; 4, conversion gap; 5, induction gap.

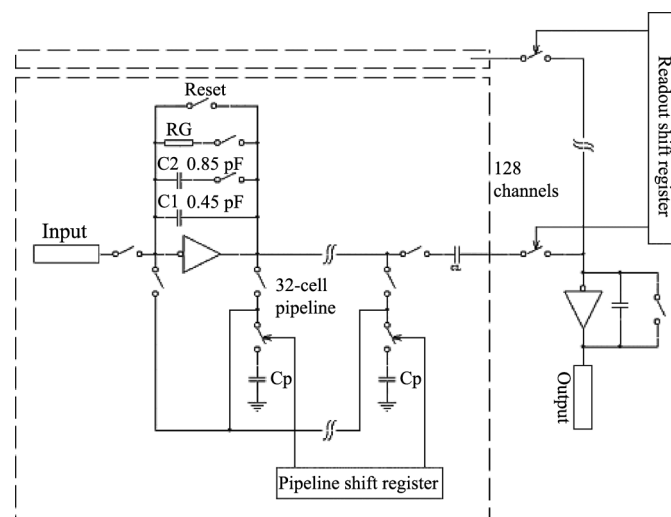


Figure 2
Schematics of the APC128 ASIC.

† Presented at the 'XIV Russian Synchrotron Radiation Conference SR2002', held at Novosibirsk, Russia, on 15–19 July 2002.

Table 1
Parameters of different regimes for APC128 operation.

	Feedback capacitor		
	C1	C1 + C2 measurement, C1 readout	C1 + C2
Noise equivalent charge (electrons)	1270	1490	1910
Maximum signal (electrons)	0.25×10^6	0.72×10^6	2.3×10^6
Maximum signal-to-noise ratio	190	480	790

Detector operation includes several stages. An external start signal initiates the measurement sequence, when the pipeline cells are coupled in series to the output of integrators synchronously with the clock pulses. The clock frequency can be chosen depending on the particular regime (time scale of the process under study). In such a way the frames of an experimental sequence are formed. After the filling of all 32 pipeline cells the measurement sequence is stopped and the readout sequence is initiated. During the readout sequence each pipeline cell is connected to the input of the integrator with a previously reset feedback capacitor. The output of the integrators is read out through the output multiplexer. Since the input integrator is used twice, during the measurement sequence and during the readout sequence, the output signal is inversely proportional to the square of the feedback capacitor. The sensitivity and thus the dynamic range of the ASIC can be changed by connecting an additional feedback capacitor to the integrator. Reduction of the sensitivity in this case can widen the dynamic range by 3.1 and 9.7 times (the capacitor C2 can be connected only for the measurement or for all the time). Parameters of different regimes are listed in Table 1. During the measurement sequence, APC128 can operate either with a reset between individual measurements or without it.

Each of the described regimes can be chosen to fit best to a particular experiment. A block diagram of the detector electronics is shown in Fig. 3. The electronics are assembled in the gas volume. The DIMEX prototype includes two APC128 ASICs, two 14-bit ADCs, 256 kbyte RAM and PLD ALTERA EPF10K20; the latter controls all the elements and provides connectivity with the network module IP302 outside the hermetic case.

3. Experimental set-up and results

The set-up which was used for the measurements of the detector parameters and for the experiments with explosions is shown schematically in Fig. 4. It uses a white synchrotron radiation beam from the 2 T wiggler at the VEPP-3 storage ring. The set-up consists of three chambers. The first chamber contains collimators which form the necessary beam shape. The second chamber is the explosion chamber where the sample is exploded. It has beryllium windows with shock-wave reducers that protect the beam channel from the detonation wave. The third chamber contains the detector and the second collimator and an additional shutter for small-angle scattering (SAXS) experiments. Spectra from the 2 T wiggler using different filtration (thickness of explosive) for the measurements are shown Fig. 5.

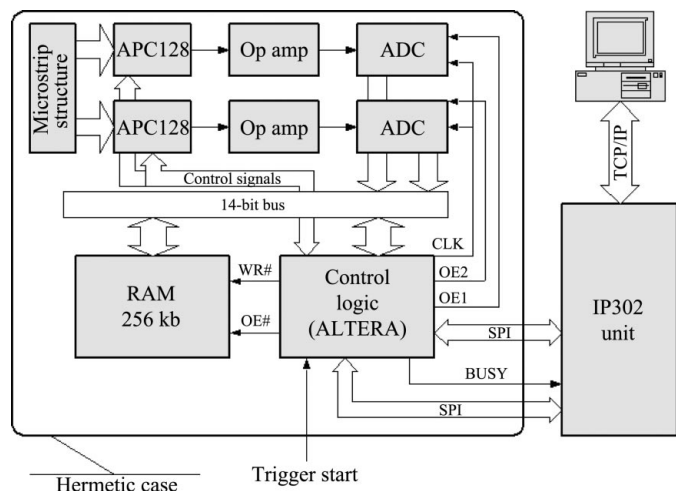


Figure 3
Block diagram of the detector electronics.

atically in Fig. 4. It uses a white synchrotron radiation beam from the 2 T wiggler at the VEPP-3 storage ring. The set-up consists of three chambers. The first chamber contains collimators which form the necessary beam shape. The second chamber is the explosion chamber where the sample is exploded. It has beryllium windows with shock-wave reducers that protect the beam channel from the detonation wave. The third chamber contains the detector and the second collimator and an additional shutter for small-angle scattering (SAXS) experiments. Spectra from the 2 T wiggler using different filtration (thickness of explosive) for the measurements are shown Fig. 5.

3.1. Spatial resolution

The spatial resolution of DIMEX is determined by secondary particles, namely photoelectrons, fluorescent photons and Auger electrons emitted after photoconversion in Xe. Because the energy is below the Xe K-edge (~ 35 keV), Auger electrons and fluorescent

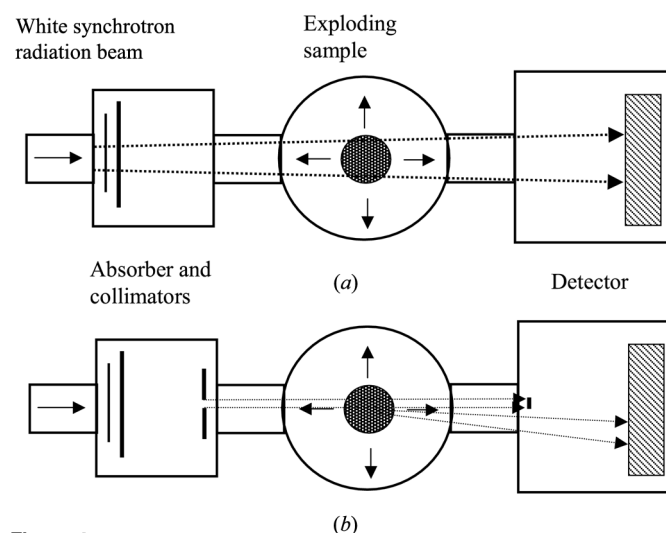


Figure 4
Schematics of the set-up for the experiments with exploding sample. (a) Set-up for the projective absorption experiments. (b) Set-up for SAXS experiments.

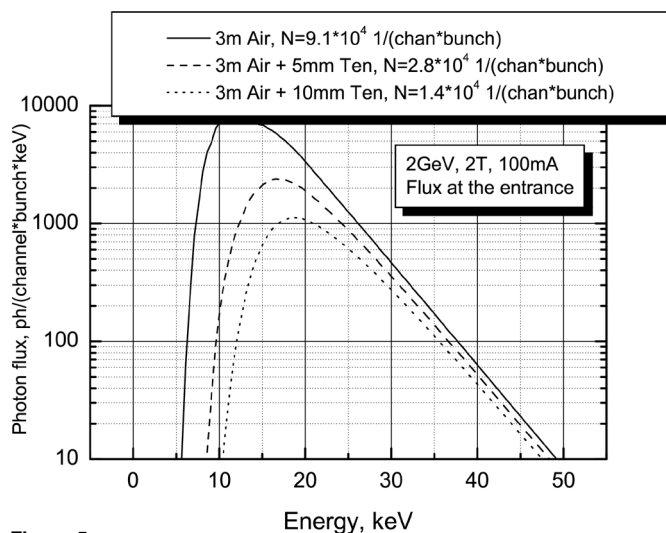


Figure 5
Energy spectrum of the beam from the 2 T wiggler. Spectra before and after 5 mm and 10 mm explosive [TEN (Russian abbreviation of penta-erythrotrinitronitrate)]. The total flux (integral over the whole energy range) is indicated as N.

photons have low energy (below 5 keV), and the spatial resolution is mainly affected by energetic photoelectrons. Transport of electrons with energy of the order of tens of keV cannot be calculated analytically so we used the *GEANT4* simulation package (Agostinelli *et al.*, 2002) to estimate the detector resolution under several experimental conditions. In Fig. 6 the line spread function (detector response for a very narrow beam) for three different gas pressures is shown. The simulation was performed for photons from an X-ray tube with a Mo target at 35 keV and took into account all relevant effects including electron diffusion. From the figure we can see that the resolution is affected by the pressure and improves from ~ 140 to ~ 110 μm (FWHM) when the pressure is increased from 5 to 15 atm.

The spatial resolution (line spread function) for the main experimental conditions with the beam from the wiggler is shown in Fig. 7. We can see that the experimental resolution at 7 atm is ~ 300 μm (FWHM) and more than twice worse than the result of the simulation. The energy spectrum of the synchrotron radiation beam has its most probable and average values very close to those of the Mo X-ray tube, and therefore this result indicates that *GEANT4* in this range of energies is not well tuned.

3.2. Time resolution

The most critical parameter of the detector is the time resolution. In order to obtain really independent images from individual electron bunches the time resolution has to be better than the bunch-crossing time. For VEPP-3 this time is equal to 250 ns in the single-bunch mode. The time resolution is determined by the electron drift velocity, beam height and the accuracy of the distance from the beam plane to the GEM plane. Longitudinal diffusion of electrons also slightly affects the resolution.

In order to measure the time resolution the detector was operated at a clock period of 125 ns, which is equal to half the bunch-crossing time. In such a case the detector is irradiated only within one out of two successive clock periods. With such a short clock period DIMEX can be operated only in the regime without the reset, as the latter is not fast, requiring ~ 150 ns. Thus, in an ideal case the dependence of the signal *versus* time must appear as 'steps' with widths of two clock periods. The difference between the ideal case and the real case provides information about the real time resolution.

The dependence of the fraction of charge collected within 125 ns after the bunch crossing as a function of reduced electric field is shown in Fig. 8 for four different measurement conditions. Open

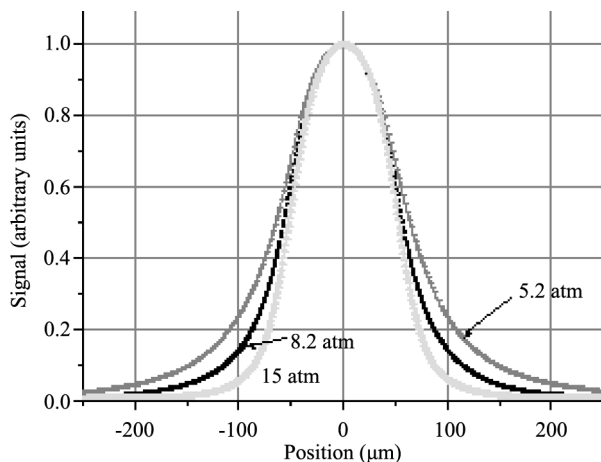


Figure 6
Line spread function for three different pressures of Xe, simulated with *GEANT4*. X-rays are from a Mo tube at 35 keV.

squares and open circles correspond to a different photon flux, 540 photons per channel and 220 photons per channel. As we will see below, at higher rates the space charge effects cause some field distortion that affects the charge collection time. In Fig. 8 the result of the calculation is also plotted. The calculation has taken into account the thickness of the 1 mm beam, the electron drift time in the gap below the GEM and the time constant of the integrator.

From the comparison of the experimental result with the calculation we see that the charge collection time is significantly underestimated. Most probably this is due to the misalignment of the detector with respect to the beam axis and more studies are needed to understand this effect. Even at this stage, however, we can state that at a reduced field of $1.8 \text{ kV cm}^{-1} \text{ atm}^{-1}$ the fraction of charge collected within 125 ns is more than 0.75. Assuming an exponential dependence of the signal *versus* time we obtain 95% charge collection in 250 ns.

3.3. Signal, noise, efficiency

The accuracy of the measurements is determined by the fraction of the primary beam absorbed by the detector (efficiency), saturation

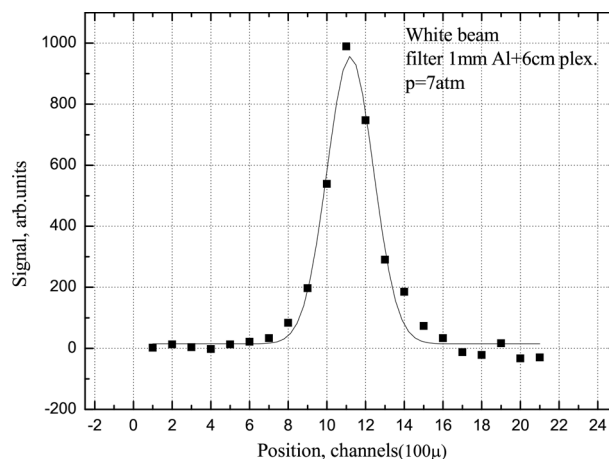


Figure 7
Line spread function measured for the beam from the 2 T wiggler. The detector is at a pressure of 7 atm.

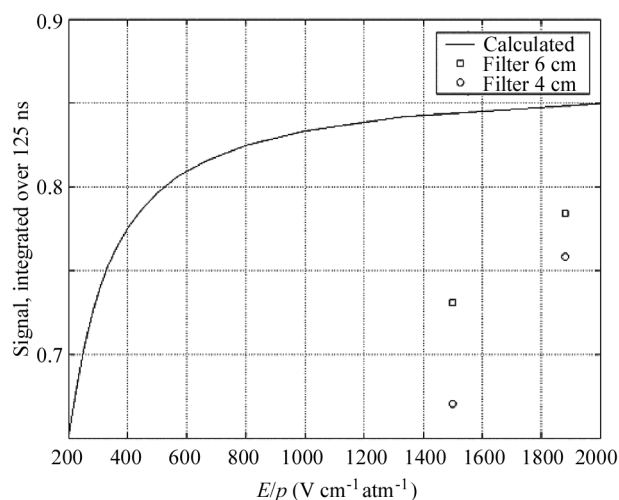


Figure 8
Fraction of charge collected within 125 ns after the bunch crossing as a function of reduced electric field. Experimental results correspond to different photon fluxes: 540 photons per channel (4 cm plexiglass filter) and 220 photons per channel (6 cm plexiglass filter).

and other distortions of the signal (noise value). We can distinguish the following noise components: electronic noise (noise without any irradiation), statistical fluctuations due to the limited number of photons detected (quantum noise) and fluctuations of the signal from the individual photon.

In Fig. 9 the calculated efficiency as a function of energy is shown for several sizes of the dead zone before the sensitive region for a detector filled with a 7 atm XeCO₂ (80–20%) mixture. The length of the sensitive region is 30 mm. In the prototype the dead zone has a length of 3 mm and the efficiency is close to 60% in the energy range around 20 keV.

The signal height from the detector as a function of X-ray flux (calculated) at the entrance window is shown in Fig. 10. Here the results of the measurements in two regimes are presented, with low and high feedback capacitance. The clock period was 500 ns (frame size) and the second bunch in the frame was masked by the reset signal. In both regimes the saturation of the signal is clearly observed at approximately the same photon flux of ~400 photons per channel. This value is strongly affected by the electric field, which indicates the space charge nature of the effect. Slow ions are accumulated in the conversion gap and distort the field such that electrons cannot be effectively transported.

One of the convenient parameters for characterization of the precision of signal measurement is the signal-to-noise ratio. For the counting detector without intrinsic noise the value of the signal-to-noise ratio (S/n) is limited by Poisson statistics and can be calculated through a simple relation with the efficiency (ϵ) and input flux (N_{in}), *i.e.* $(S/n)^2 = \epsilon N_{in}$. The square of the signal-to-noise ratio is called the noise equivalent quanta (NEQ), as this is the number of photons that make the statistical fluctuations equal to the total noise of the detector. The NEQ as a function of input flux for the same two regimes as in Fig. 10 is shown in Fig. 11. The NEQ for the case of a 100% efficient counting detector (Poisson limited detector) is shown in the figure as a dashed line. The ratio of the NEQ for a particular case and that for the ideal detector gives a value of the detective quantum efficiency (DQE). For the regime with low feedback capacitance DQE is equal to ~50%, while that for the regime with high feedback capacitance is much lower. This is due to some additional electronic noise appearing during the measurement under real experimental conditions. This additional noise source will be investigated during further studies.

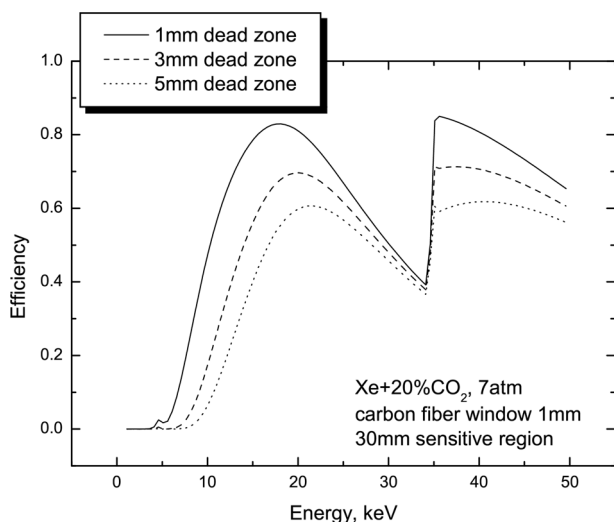


Figure 9 Efficiency as a function of energy for different lengths of the dead zone in front of the sensitive region. The gas pressure is 7 atm.

4. Discussion and conclusions

In the present work we have demonstrated that the concept of a very fast detector for imaging, using synchrotron radiation flashes from individual bunches, can be realised. The first prototype of DIMEX has shown a spatial resolution of ~300 μm (FWHM), a time resolution of ~100 ns and a dynamic range of ~15. The maximum detected photon rate before saturation was ~200 photons per channel per bunch. This value corresponds to a photon flux of ~10¹⁰ mm⁻² s⁻¹. The dynamic range and maximum photon flux are limited by space charge effects and additional electronic noise produced during operation of the APC128 chip in a regime with a high frame rate. The solutions of these problems can allow an improvement of the dynamic range of up to ~50 and maximum photon rate up to ~2000 photons per channel per bunch. These values are determined only by the APC128 properties, and further improvements will be possible only through the development of a new ASIC.

Even with the present moderate dynamic range the first experiments with exploding samples have shown the great potential of the techniques. By performing several experiments under identical

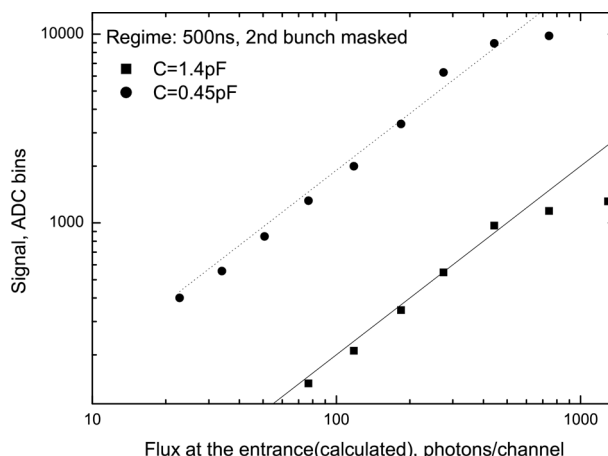


Figure 10 Signal as a function of X-ray flux per channel at the entrance window of the detector under the real experimental conditions. Results are shown for the regimes with high and low feedback capacitance.

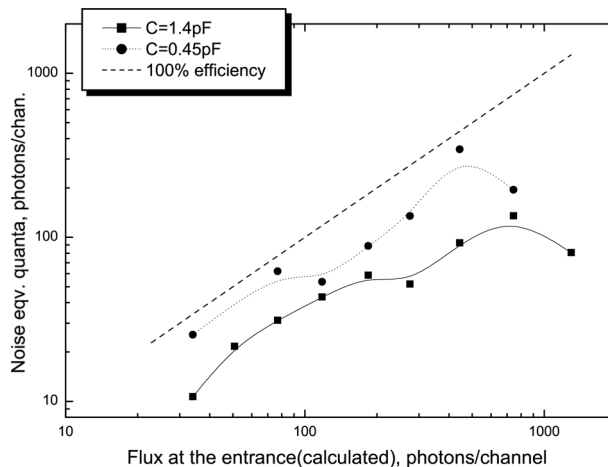


Figure 11 NEQ as a function of input flux. Results are shown for the regimes with high and low feedback capacitance.

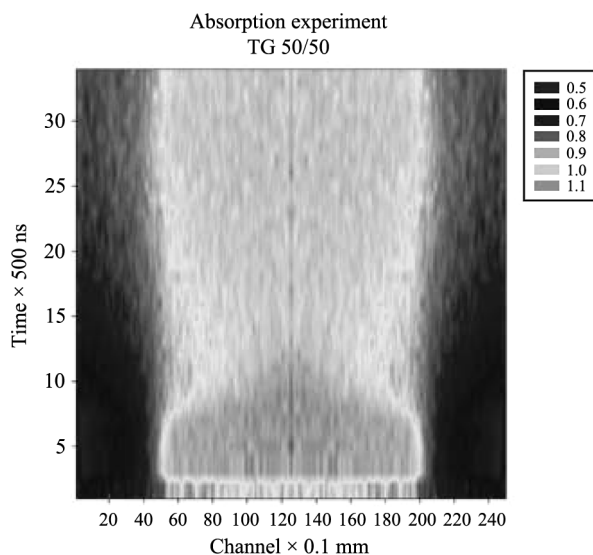


Figure 12

Result of the series of projective absorption experiments (ten explosions). Horizontal axis: position in channels ($100\ \mu\text{m}$); vertical axis: time in units of 500 ns.

conditions and synchronization we could improve the accuracy by the addition of several images. In Fig. 12 the result of a series of ten projective absorption experiments is shown. The figure demonstrates

clearly the detonation front, high-density reaction zone after the detonation wave, and decay of the explosion products afterwards. The projective absorption experiments have shown the ability of the method to improve significantly the information needed for the precise hydrodynamic model of the explosion and to provide new knowledge about the structure of the reaction zone. More details about the results of the first experiments are presented by Titov *et al.* (2002).

The authors would like to thank very much Roland Horisberger, who provided APC128 ASICs and all relevant information.

References

- Agostinelli, S. *et al.* (2002). *GEANT4 – A Simulation Toolkit*. CERN-IT-2002-003. CERN, Geneva, Switzerland.
- Aleshaev, A. N., Batrakov, A. M., Fedotov, M. G., Kulipanov, G. N., Lukjanchikov, L. A., Ljachov, N. Z., Mishnev, S. I., Sheromov, M. A., Ten, K. A., Titov, V. M., Tolochko, B. P. & Zubkov, P. I. (2001). *Nucl. Instrum. Methods*, **A470**, 240.
- Horisberger, R. & Pitzl, D. (1993). *Nucl. Instrum. Methods*, **A326**, 92–99.
- Sauli, F. (1997). *Nucl. Instrum. Methods*, **A386**, 531–534.
- Titov *et al.* (2002). XIV Russian Synchrotron Radiation Conference SR2002, Novosibirsk, Russia, on 15–19 July 2002.
- Tolochko, B. P., Aleshaev, A. N., Fedotov, M. G., Kulipanov, G. N., Lyakhov, N. Z., Luk'yanchikov, L. A., Mishnev, S. I., Sheromov, M. A., Ten, K. A., Titov, V. M. & Zubkov, P. I. (2001). *Nucl. Instrum. Methods*, **A467/468**, 990–993.